Environmental Science & Technology

Article

Cite This: Environ. Sci. Technol. 2018, 52, 12895−12904

pubs.acs.org/est

Impact of Haloarchaea on Speciation of Uranium—A Multispectroscopic Approach

Miriam Bader,[†] André Rossberg,[†] Robin Steudtner,[†] Björn Drobot,[†,‡] Kay Großmann,[†] Matthias Schmidt,[§] Niculina Musat,[§] Thorsten Stumpf,[†] Atsushi Ikeda-Ohno,[†] and Andrea Cherkouk*[,†]

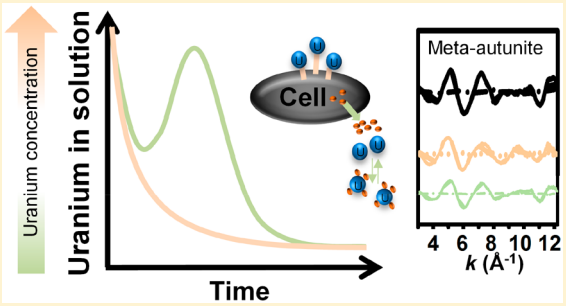
[†]Helmholtz-Zentrum Dresden-Rossendorf, Institute of Resource Ecology, Bautzner Landstraße 400, 01328 Dresden, Germany

[‡]Technische Universität Dresden, Central Radionuclide Laboratory, Zellescher Weg 19, 01062 Dresden, Germany

[§]Helmholtz Centre for Environmental Research, Department of Isotope Biogeochemistry, Permoserstraße 15, 04318 Leipzig, Germany

Supporting Information

ABSTRACT: Haloarchaea represent a predominant part of the microbial community in rock salt, which can serve as host rock for the disposal of high level radioactive waste. However, knowledge is missing about how Haloarchaea interact with radionuclides. Here, we used a combination of spectroscopic and microscopic methods to study the interactions of an extremely halophilic archaeon with uranium, one of the major radionuclides in high level radioactive waste, on a molecular level. The obtained results show that *Halobacterium noricense* DSM 15987^T influences uranium speciation as a function of uranium concentration and incubation time. X-ray absorption spectroscopy reveals the formation of U(VI) phosphate minerals, such as meta-autunite, as the major species at a lower uranium concentration of 30 μM, while U(VI) is mostly associated with carboxylate groups of the cell wall and extracellular polymeric substances at a higher uranium concentration of 85 μM. For the first time, we identified uranium biomineralization in the presence of *Halobacterium noricense* DSM 15987^T cells. These findings highlight the potential importance of Archaea in geochemical cycling of uranium and their role in biomineralization in hypersaline environments, offering new insights into the microbe-actinide interactions in highly saline conditions relevant to the disposal of high-level radioactive waste as well as bioremediation.



INTRODUCTION

Uranium is present in high inventory in high level radioactive waste, for example, through the production of enriched nuclear fuels or as a byproduct of fuel reprocessing.[1] In the environment it is mainly present in the two major oxidation states of U(VI) and U(IV). Rock salt can serve as a potential host rock for the geological disposal of high level radioactive waste because of its properties as, for example, high temperature conductivity, impenetrability, and viscous deformation behavior. It consists mainly of halite with other components including carbonates, anhydrite or gypsum, and chloride or sulfate salts of magnesium and potassium.[2] Some of these components are known to be poorly uraniferous minerals. Therefore, the rock salt has a low intrinsic capacity to retard uranium. In rock salt Haloarchaea represent a dominant part of the microbial community.[3,4] Microorganisms indigenous to those host rock environments have a potential impact on the mobility and retardation of radionuclides via, for example, biosorption, bioaccumulation, biotransformation, and biomineralization.[5−7] The formation of uranium-containing phosphate minerals by bacteria, fungi, and a few Archaea, was reported where meta-autunite-like minerals were formed.[8−13] Thus far, only a limited number of studies have been reported about the biosorption of actinides on halophilic archaea. Sorption of Cm(III) onto cells of *Halobacterium salinarum* ATCC 19700^T was shown to be a fast process, which reached equilibrium after 20 min.[14] The association of uranium with a member of the family *Halobacteriacea*, namely *Halobacterium halobium* ATCC 43214^T (renamed as *Halobacterium salinarum*[15]), was studied in relation to other halophilic and nonhalophilic bacteria,[11] where an extracellular accumulation of uranium was observed as dense deposits.

In order to assess the potential implication of *Halobacterium* species on the chemical behavior of metals including uranium, more precise knowledge of the interaction between *Halobacterium noricense* DSM 15987^T and uranium is fundamental on a molecular level. Such knowledge is essential to assess the potential migration of actinides in the presence of indigenous microorganisms in hypersaline environments to better predict

Received: May 18, 2018
Revised: July 20, 2018
Accepted: August 20, 2018
Published: August 20, 2018

Downloaded via LOS ALAMOS NATL LABORATORY on January 11, 2019 at 21:46:13 (UTC).
See https://pubs.acs.org/sharingguidelines for options on how to legitimately share published articles.

© 2018 American Chemical Society

DOI: 10.1021/acs.est.8b02667
Environ. Sci. Technol. 2018, 52, 12895−12904

the safety of a potential nuclear waste repository in rock salt and to improve the utilization of Haloarchaea for development of bioremediation strategies of metal-contaminated environments.[16]

Extremely halophilic Archaea belonging to the genus *Halobacterium* were detected by both cultivation-dependent and cultivation-independent studies in rock salt worldwide.[4,17−20] This study focuses on *Halobacterium noricense* DSM 15987^T, which was originally isolated from a bore core of a salt mine in Altaussee, Austria.[17] Closely related strains and species were also isolated from other ancient rock salts,[4,20] suggesting this *Halobacterium* species would be a good representative of a rock salt indigenous archaeon.

The aim of the present study was to provide a comprehensive overview of the interaction mechanisms between *H. noricense* DSM 15987^T and uranium on a molecular level. The obtained results will identify the uranium species formed in the presence of *H. noricense* DSM 15987^T cells under different conditions by a combination of microscopic and spectroscopic methods.

MATERIALS AND METHODS

Cultivation of Haloarchaeal Cells. *H. noricense* DSM 15987^T was purchased from the Leibniz Institute DSMZ - German Collection of Microorganisms and Cell Cultures (DSMZ, Braunschweig, Germany). The strain was cultivated as recommended in DSM372 medium, pC_{H+} 7 (per L: 200 g NaCl, 5 g yeast extract, 5 g casamino acids, 1 g KCl, 20 g $MgSO_4 \cdot 7H_2O$, 3 g Na_3-citrate, 1 g Na-glutamate, 36 mg $FeCl_2 \cdot 4H_2O$, 0.36 mg $MnCl_2 \cdot 4H_2O$, replacing $MnCl_2 \cdot 4H_2O$, to $MgCl_2 \cdot 6H_2O$ for an accelerated growth) under aerobic conditions. During growth, the cells were shaken at 140 rpm in a water bath at 30 °C in the dark. Cells of *H. noricense* were harvested during exponential growth (OD_{600} of about 0.55, day 4 of growth) by centrifugation at 10 000*g* and 18 °C for 10 min. The harvested cells were washed three times with 3 M NaCl at pC_{H+} 6 prior to the following experiments.

Batch Experiments to Study Bioassociation of Uranium. The experimental setup was designed to study the biosorption of uranium on archaeal resting cells. A defined amount of *H. noricense* biomass (0.5 mg dry biomass (DBM) per mL) was used for batch experiments. A DBM of 0.5 mg per mL was defined according to a linear relation to the OD_{600} of the cell suspension of 0.27. Cell pellets gained after centrifugation from 1 mL of washed cell suspension were used to monitor DBM by weighing triplicate samples after drying for 48 h at 70 °C.

Given the high ionic strength of 3 M NaCl, the measured pH (negative logarithm of the hydrogen ion activity), which was adjusted with 0.1 M HCl to 5.51, was corrected by a factor of 0.49 to obtain the hydrogen ion concentration pC_{H+}.[21,22] The original uranium compound of $UO_2(NO_3)_2 \cdot 6H_2O$ was obtained from Chempol, Praha/Lachema, Czech Republic. The compound was converted to UO_3 in a muffle furnace at 320 °C,[23] and the resultant UO_3 was dissolved in 0.5 M HCl to obtain a uranium stock solution with a concentration of 78 mM U(VI). Uranium solutions for batch experiments (30 and 85 μM U(VI), pC_{H+} 6.) were filter-sterilized (pore size 0.2 μm Filtropur Sarstedt) before use. The absence of colloidal particles in the solutions was proven by dynamic light scattering. The cell pellet was resuspended in 10 mL of filter-sterilized 3 M NaCl solution containing U(VI), at pC_{H+} 6. Batch experiments were carried out in 50 mL plastic tubes. The triplicated sample tubes were shaken at 150 rpm at room temperature, in the dark. Time-dependent bioassociation studies with U(VI) were performed at certain time points within the time frame of 5 min up to 2 weeks (Supporting Information (SI) Table S1), whereas for each time point separate triplicates were setup. After incubation, the cell suspensions of *H. noricense* were centrifuged (18 °C, 10 000*g*, 10 min) to separate supernatant from cell pellet. The uranium concentration in the supernatant was determined with inductively coupled plasma mass spectrometry (ICP-MS; Elan 9000 PerkinElmer, Waltham, MA). Abiotic control samples without cells were treated in the same manner to exclude the effects of abiotic removal of uranium from the solution, such as precipitation and/or chemical sorption to the vials. Additionally, control samples with dead cells were treated in the same manner (see Supporting Information).

Scanning Electron Microscopy Coupled with Energy-Dispersive X-ray Analysis for Elemental Mapping. The localization of uranium on cells of *H. noricense* was investigated by scanning electron microscopy (SEM) coupled with energy dispersive X-ray spectroscopy (EDX) by using a scanning electron microscope (Zeiss Merlin VP Compact, Carl Zeiss Microscopy, Germany) coupled with an EDX detector (Bruker Quantax FlatQUAD, Bruker Nano GmbH, Germany, Berlin). The electron-acceleration energy was amounted to 5.0 kV. Cells incubated for a certain time with 30 μM U(VI) were washed once with 3 M NaCl at pC_{H+} 6, fixed with paraformaldehyde (1% paraformaldehyde in 3 M NaCl), collected on a polycarbonate filter (GTTP type, 0.2 μm pore size, Millipore, coated with a mixture of Au/Pd using a Leica EM SCD 500 sputter-coater), rinsed with 3 M NaCl at pC_{H+} 6 and dried at room temperature.

X-ray Absorption Spectroscopy. For X-ray absorption spectroscopy (XAS) studies, the cells were treated with two different U(VI) concentrations (30 and 85 μM) for different incubation times (1 h, 5 h, 48 h, 7 d, and 14 d) in the same way as employed for the batch experiments described above (SI Table S1). In total eight samples were provided. In addition to these eight samples, two samples with a U(VI) concentration of 50 μM and an incubation time of 48 h were also measured, mainly in order to improve the statistics on the mathematical treatment on the acquired XAS data, as mentioned below. Cell pellets of triplicate samples were collected after a certain incubation time by centrifugation at 10 000*g* for 10 min at 18 °C gathered in a single sample vial and washed two times with 3 M NaCl at pC_{H+} 6. Afterward the cell pellet was transferred as wet paste in a 3 mm thick polyethylene sample holder double confined with Kapton tape and polyethylene.

X-ray absorption spectra, including both X-ray absorption near-edge structure (XANES) and extended X-ray absorption fine structure (EXAFS) regions, were collected at U L_{III}-edge (17185 eV) on the Rossendorf beamline (ROBL, BM20) at the European Synchrotron Radiation Facility (ESRF)[24] under dedicated ring operating conditions of 6 GeV and 200 mA. A Si(111) double-crystal monochromator was used in the channel-cut mode to monochromatize incident white X-rays and higher order harmonics were rejected by two Rh-coated mirrors. The X-ray absorption data were collected at ambient pressure and temperature in fluorescence mode using a gas filled (86% N_2, 14% Ar) ionization chamber for monitoring the incident X-ray intensity and a 13-element Ge solid state detector (Canberra) for monitoring the fluorescence X-ray intensity. Energy calibration of the acquired spectra was

DOI: 10.1021/acs.est.8b02667
Environ. Sci. Technol. 2018, 52, 12895−12904

performed by the simultaneous measurement of Y K-edge of a reference Y foil, the first inflection point of which is defined at 17038 eV. Up to 11 scans were performed for a single sample and the data were averaged for data analysis. The acquired X-ray absorption spectra were treated according to a standard procedure[25] on the programs EXAFSPAK[26] and WinXAS.[27] The treated XAS data were further analyzed by iterative transformation factor analysis (ITFA) and target transformation factor analysis (TFA), which are described in detail in SI.

Cryo Time-Resolved Laser-Induced Fluorescence Spectroscopy. Cryo time-resolved laser-induced fluorescence spectroscopy (TRLFS) with an excitation wavelength (λ_{exc}) of 266 nm was used to investigate the speciation of uranium in the samples prepared in the same way as for XAS. The combined cell pellet was collected in a sample holder developed for solid phase cryo measurements. Supernatants of the samples and U(VI) references were measured in a disposable plastic UV-cuvette at −120 °C. The experimental setup for luminescence data collection was reported elsewhere[28,29] apart from the applied laser energy (0.8 mJ) and the slit width (200 μm). A dynamic step width in the range from 0.1 to 12 502 μs was used to detect species with a longer emission lifetime as well as species with shorter emission lifetimes. Spectra were averaged over 100 accumulations and the baseline was corrected with the software LabSpec 5 (Horiba). Stacking of the collected TRLFS data gave a 16 × 50 × 300 data array (samples × time × wavelength). The data were analyzed with parallel factor (PARAFAC) analysis using the N-way toolbox[30] with Matlab R2015a. Individual luminescence lifetimes were constraint to monoexponential decay.[28]

Cryo Fluorescence Microscopy Coupled with Laser-Induced Fluorescence Spectroscopy. The cells incubated with 30 and 85 μM U(VI) for 7 d were studied at 28 K with a confocal microscope (Leica TCS-SP2 CLSM - Leica Microsystems, Germany) coupled to a detection device for laser-induced fluorescence spectroscopy (LIFS). The wavelength of 408 nm, generated by a continuous wave diode laser (Vioflame (408 nm/25 mW), Coherent Inc.), was chosen for excitation of uranyl(VI) and coupled into the confocal laser scanning microscope (CLSM) via the UV port. Details about the experimental setup have been described in ref 31. Cryo temperature measurements were performed by using a Cryo Micro Station chamber (CMS 3.1 Nanoscopix, Life Science-Inkubator, Dresden, Germany). The CMS 3.1 is a closed cycle refrigerator based cryostat, which is especially developed for easy microscopic measurements at very low temperatures. The influence of low pressure to the samples was inhibited by positioning coverslips on top of the samples and subsequently sealing the coverslips at the edges with nail polish (Express finish shock control, Maybelline Jade). After reaching the temperature of 28 K on the sample holder, the samples were tempered for 1 h prior to the measurements.

RESULTS

Bioassociation of Uranium. As shown in Figure 1, a multistage association was observed with an initial U(VI) concentration of 30 μM. Within the first 30 min of contact up to 27.2 ± 3.5% of the initial amount of uranium was removed from the solution (SI Table S1). This was followed by a release of uranium into the supernatant in the subsequent 4 h. The amount of uranium in the supernatant decreased afterward and eventually reached 21.3 ± 0.2% after 40 h. When the contact time was further prolonged up to 14 days, a slight decrease

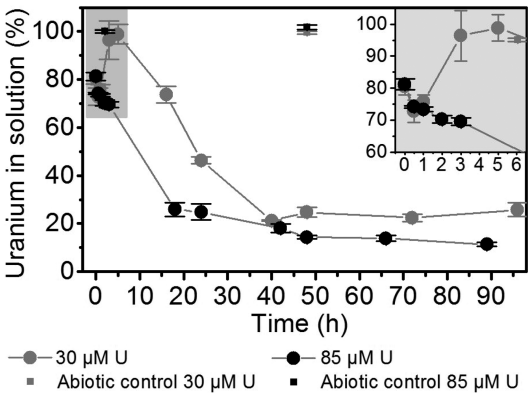


Figure 1. Uranium content in supernatant after contact with *Halobacterium noricense* DSM 15987^T cells for different periods of time (pC_{H+} = 6, DBM = 0.5 mg/mL, [NaCl] = 3 M, (gray circles: living cells, [U(VI)] = 30 μM; gray squares: abiotic control, [U(VI)] = 30 μM; black circles: living cells, [U(VI)] = 85 μM; black squares: abiotic control, [U(VI)] = 85 μM)). Inset figure in gray at the top-right is the enlargement for a shorter contact time (~7 h).

down to 6.9 ± 0.1%, which corresponds to 3.7 mg uranium per g DBM (mg_U/g_{DBM}), was observed. On the other hand, at a higher initial uranium concentration of 85 μM, such a multistage association was not observed and the amount of uranium in the supernatant decreased continuously to 14.3 ± 0.7% within 48 h (Figure 1), which corresponds to 44.6 mg_U/g_{DBM}, and reached a plateau. In contrast, when dead cells were used, the uranium content in the supernatant decreased down to 12.4 ± 1.9% within the first 5 h (SI Figure S1). Cells incubated with or without uranium were stained with the two dyes SYTO 9 (green fluorescence, viable cells) and propidium iodide (red fluorescence, nonviable cells) to get information about the cell viability. Cells of *H. noricense*, incubated without uranium in 3 M NaCl, were mostly alive and single for up to 14 days with a slight decrease in cell numbers (SI Figure S2). The cells treated with a lower uranium concentration of 30 μM were also mostly alive for up to 14 days. However, the formation of small agglomerates was observed after 48 h and the size of the agglomerates increased with increasing incubation time. The cells treated with a higher uranium concentration of 85 μM agglomerated immediately and the size of the agglomerates increased further with increasing incubation time. As shown in SI Figure S2, the number of dead cells (red) increased with increasing incubation time as well as increasing uranium concentration. This indicates that the cells did not tolerate higher uranium concentrations.

Localization of Uranium by SEM Coupled with EDX. Selected samples from the batch experiments of *H. noricense* with 30 μM U(VI) were analyzed by SEM coupled with EDX to gain information about the localization of uranium. Due to a lower amount of U(VI) associated with the cells, the mapping of uranium for the samples with an incubation time of less than 24 h was not possible. However, differences are obvious by comparing micrographs from samples incubated for 24 h and 96 h (Figure 2). Sodium chloride crystals were observed in all sample images due to the highly saline conditions. After 24 h, single cells were visible and they are covered with mineral-like phases. The results of elemental mapping showed that uranium is mainly associated with the cells and incorporated in the mineral-like phases covering the cells. After 96 h, small agglomerates were observed and uranium was associated with the cells. Additionally, uranium was also detected within extracellular

DOI: 10.1021/acs.est.8b02667
Environ. Sci. Technol. 2018, 52, 12895−12904

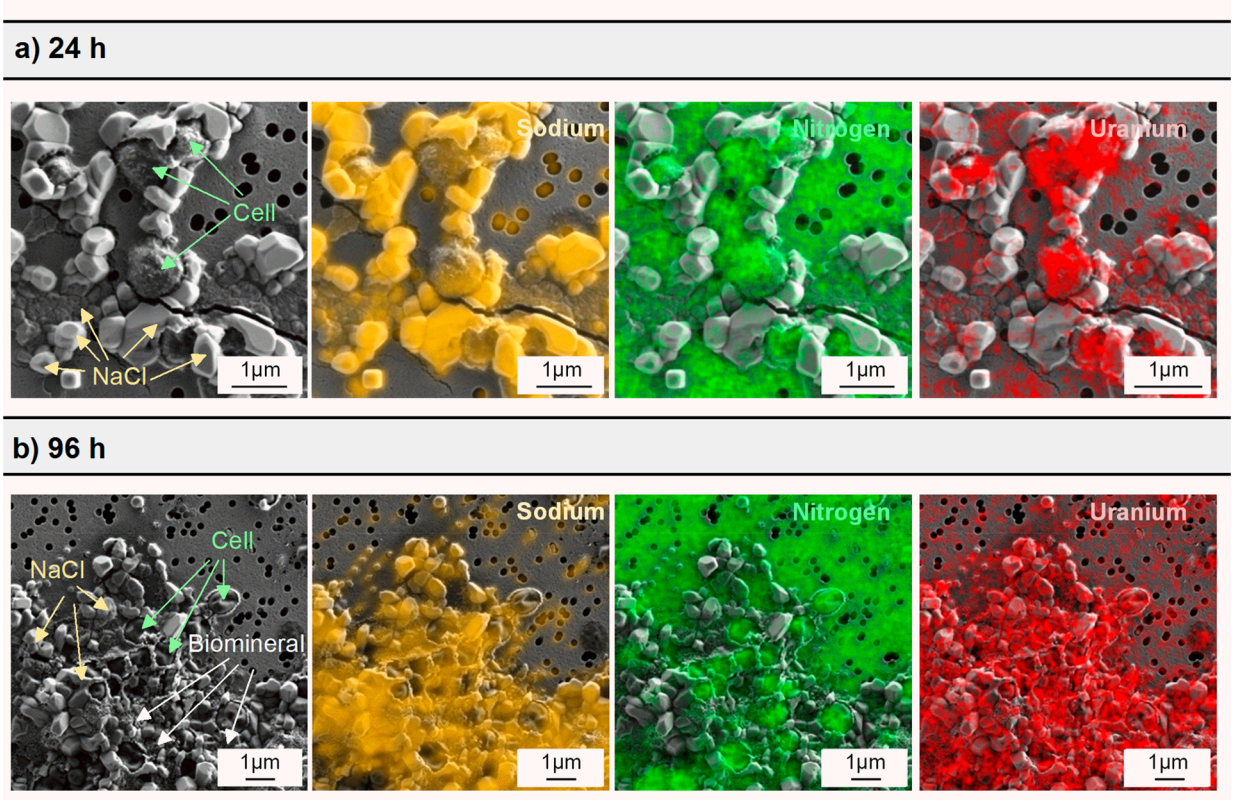


Figure 2. Scanning electron microscopy images of *Halobacterium noricense* DSM 15987^T cells treated with uranium ([U(VI)] = 30 μM, pC_{H+} 6, [NaCl] = 3 M) for (a) 24 h and (b) 96 h. The colored images are overlays of SEM and mapping data from EDX spectroscopy.

substances as biomineral-like phases (SI Figure S3). The high resolution microscopy image (recorded with Helium ion microscope) showed that the cell surface is still intact even after 96 h in the presence of uranium (SI Figure S4). This indicates that there is no change in cell morphology under the experimental conditions.

Speciation of Bioassociated Uranium by X-ray Absorption Spectroscopy. ITFA on a series of the acquired XANES data calculates two significant eigenvectors (SI Figure S5), indicating that the spectra can be interpreted with two components, that is, two different oxidation states are present in the series of the samples. The linear combination of the two eigenvectors reasonably reproduces all measured XANES spectra as shown in Figure 3a and SI Figure S6. On the other hand, ITFA on the U L_{III}-edge EXAFS spectra results in three significant eigenvectors (SI Figure S7), indicating that there are at least three independent U species in the series of the samples. All EXAFS spectra can be reasonably reproduced by the linear combination of these three eigenvectors (Figure 3b and SI Figure S8). In order to identify the most reasonable references for further analyzing the acquired EXAFS spectra, target transformation (TT) analysis was performed on a series of U L_{III}-edge EXAFS spectra for U(IV) and U(VI) compounds listed in SI Table S2 containing possible U minerals and several U(VI) complexes with 13 structurally different aliphatic (hydroxy)carboxylic acids at different pH values. For the U(IV) references, a U(IV) carbonate compound ($Na_6[U^{IV}(CO_3)_5]$),[32] and a U(IV) aquo complex ($U_{IV}(H_2O)_n$)[33] provide SPOIL values lower than 3 (SI Table S2), which can be acceptable targets according to the Malinowski's well-merited appreciation.[34] Because of the solid form of the samples, the U(IV) aquo complex is unlikely to be present in the samples. Other U(IV) compounds, such as UO_2, provide SPOIL values far exceeding 3 and are not suitable to be considered as acceptable targets. Hence, it is reasonable to select the U(IV) carbonate complex as an appropriate U(IV) reference. For U(VI) references, carbonates, inorganic(as meta-autunite) and organic phosphates (U(VI) complexes with fructose-1,6-bisphosphate and with DNA), and carboxylates can be considered. Among a series of these U(VI) references, a phosphate compound of meta-autunite shows a low SPOIL value of 1.86 and, hence, can be considered as a promising target (SI Table S2). In addition to meta-autunite, aqueous U(VI) tricarbonate complexes and a carboxylate complex with lactate result in SPOIL values lower than 3. However, given the solid form of the samples, aqueous U(VI) carbonate species are unlikely. On the other hand, there is an indication of the interaction of U(VI) with the carboxylate groups of cell envelope or secreted organic compounds from the cryo-TRLFS investigations. As a matter of fact, glycoconjugates as *N*-acetylneuraminic acid (NANA) with a multidentate functional group composed of a α-hydroxy acid were detected in biofilm structures of *Halobacterium salinarum* DSM 3754^T.[35] The α-hydroxy acid motif within NANA is comparable to the coordination geometry of lactate (i.e., one hydroxyl and one carboxylate group). Therefore, the U(VI) lactate complex, which represents a polynuclear species at the studied pH,[36] would be a more appropriate reference than the U(VI) carbonates. Given these facts, the three selected references, that is, U(IV)-carbonate, meta-autunite, and U(VI)-lactate are used to estimate their fractions in the EXAFS spectra by ITFA and TFA (SI Table S4).

In the case of the XANES spectra, the two detected components can be assigned to U(IV) and U(VI), which is in

DOI: 10.1021/acs.est.8b02667
Environ. Sci. Technol. 2018, 52, 12895−12904

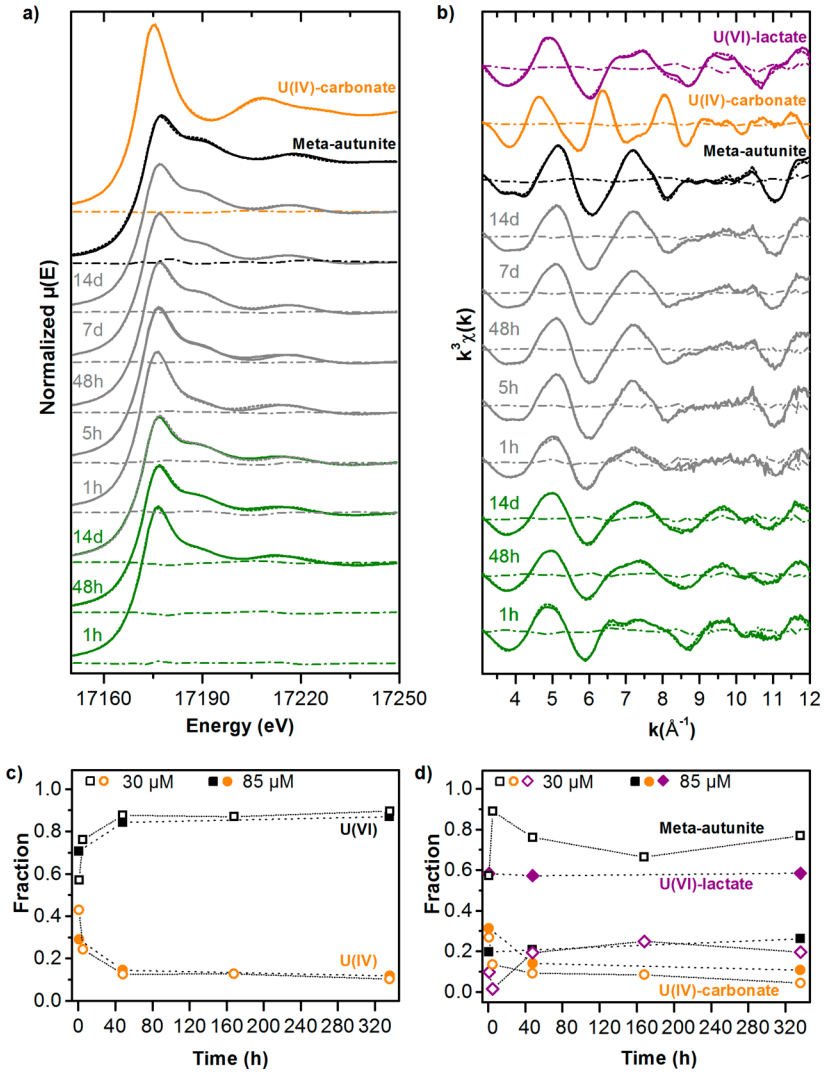


Figure 3. (a) Normalized U L_{III}-edge XANES spectra and (b) k^3-weighted U L_{III}-edge EXAFS spectra of samples with different uranium concentrations (gray: [U(VI)] = 30 μM, green: [U(VI)] = 85 μM) and different incubation times together with the reference compounds U(IV)-carbonate ($Na_6[U(CO_3)_5]$)[32] (orange), U(VI)-lactate (purple) and meta-autunite (black). Solid lines: experimental data, dotted lines: reproduction by iterative transformation factor analysis (ITFA) based on two and three principal components (i.e., eigenvectors) for XANES and EXAFS, respectively, and dashed dotted lines: residual between experimental data and ITFA reproduction. (c) Fractions of the U(VI) (black) and U(IV) species (orange) calculated by ITFA from the XANES spectra, and (d) fractions of three major species calculated by ITFA on EXAFS spectra, corresponding to meta-autunite (black), U(VI)-lactate (purple) and U(IV)-carbonate (orange), respectively.

line with the fact that neither U(III) nor U(V) are expected to be stable in the conditions of our samples.[37] Hence, in order to calculate the fractions of these oxidation states by TFA, U(IV)-carbonate and meta-autunite are appropriate references for U(IV) and U(VI), respectively. The U(IV) and U(VI) fractions calculated by ITFA on XANES are given in Figure 3c and SI Table S3. The samples with the shortest incubation time of 1 h exhibit high fractions of U(IV) at both concentrations, which decreased as a function of incubation time. In addition to the information about the oxidation states derived from the XANES data, speciation information can be acquired from the EXAFS spectra. ITFA and TFA calculate the fractions of the components based on different algorithms. The fractions determined by ITFA and TFA show similar trends (SI Table S4), suggesting the reliability of the obtained information on speciation distribution. The calculated fractions based on the EXAFS spectra are well comparable to those derived from the XANES data (Figure 3c and Figure 3d), further supporting the validity of the ITFA/TFA results both on the XANES and EXAFS spectra. The results show that meta-autunite is the major fraction in the samples with the lower initial U(VI) concentration of 30 μM, whereas U(VI)-lactate is the major fraction in the samples with the higher initial U(VI) concentration of 85 μM (Figure 3d).

Speciation of Bioassociated Uranium by Cryo Time-Resolved Laser-Induced Fluorescence Spectroscopy. The speciation of uranium associated with the cells was further investigated with cryo-TRLFS, which is complementary to XAS. The collected TRLFS data for supernatants and cell pellets (SI Figure S9) were analyzed together with PARAFAC.[38] The six extracted spectra are shown in Figure 4 together with their appropriate reference spectra. An assignment was made based on the comparison of peak positions and ratios with those for the corresponding references. The two detected spectra in the supernatant can be assigned to aqueous U(VI) species. Spectrum 1 can be assigned to a polynuclear 3:5 U(VI) hydroxo complex

DOI: 10.1021/acs.est.8b02667
Environ. Sci. Technol. 2018, 52, 12895−12904

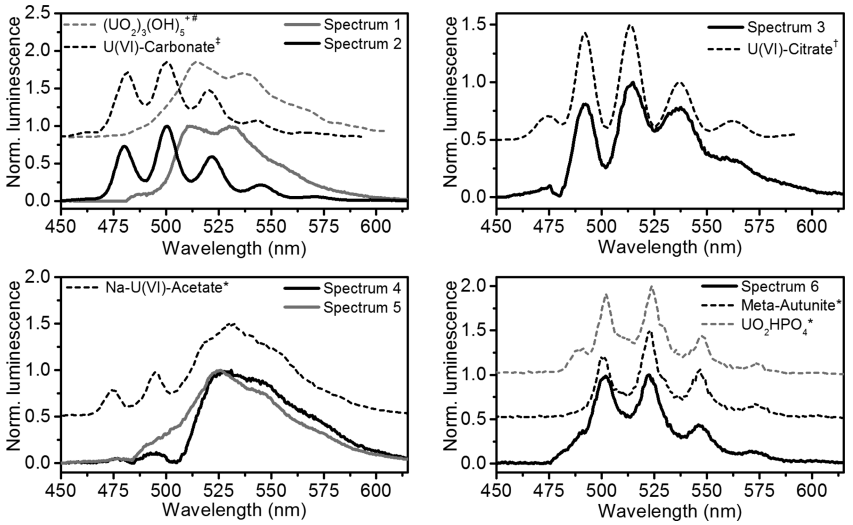


Figure 4. Luminescence spectra of six major components extracted by parallel factor (PARAFAC) analysis on the acquired TRLFS data (solid lines), together with the spectra for corresponding reference species (dashed lines, * this work, † data taken from ref 29, # data taken from ref 39, ‡ data taken from ref 41).

$((UO_2)_3(OH)_5^+)$,[39] which is dominating the abiotic blank, and spectrum 2 to the U(VI) tricarbonate complex $(UO_2(CO_3)_3^{4-})$.[40,41] Spectrum 2 was not detected in the abiotic blank and occurred only in the supernatant (SI Figure S9b). Hence, the formation of the uranyl carbonate species could originate from the release of CO_2 by the microorganisms. The release of CO_2 is followed by the dissolution of CO_2 to form a carbonate species, which is a strong complexing ligand for uranium.[42] In the cell pellets, four different spectra were detected. Spectra 3–5 can be assigned to U(VI) species complexed with carboxylate functions. In particular, spectrum 3 showed a high similarity to U(VI)-citrate.[29] Spectra 4 and 5 can be assigned to U(VI)-acetate and are supposed to be polynuclear complexes.[43−45] Spectrum 6 can be assigned to U(VI)-phosphates (Figure 4). The distribution of the identified species over the experiment duration is shown in SI Figure S10. It should be noted that the luminescence emission intensity of uranyl(VI) species can differ among different species due to the different quantum yields or the differences in excitation wavelength.[38,46] Hence, the luminescence emission intensity is not directly reflecting their real fraction. For example, the high quantum yield of carbonate species lead to the overestimation of this fraction by TRLFS.

The localization of uranium on the archaeal cells after 1 week of incubation was further studied by cryo fluorescence microscopy (CFM) coupled with LIFS. Blue color in fluorescence micrographs of Figure 5b represents uranyl(VI)-induced luminescence, showing a wide distribution over the agglomerates. Information about the U(VI) speciation can be further obtained by analyzing the luminescence spectra. The obtained spectra shown in Figure 5a are in good agreement with the original spectra from the cryo-TRLFS measurements (SI Figure S9) regarding its band positions.

DISCUSSION

The results from EXAFS and luminescence spectroscopy indicate the formation of U(VI)-phosphate (meta-autunite) and U(VI)-carboxylates as well as potentially U(IV)-carbonate, a result of the interaction of the initial U(VI) species with *H. noricense* DSM 15987^T.

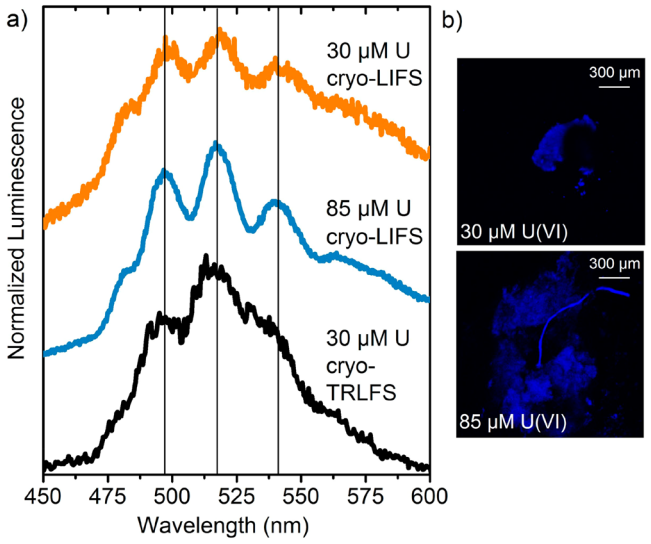


Figure 5. (a) Cryo luminescence spectra of uranyl(VI) associated with the cells incubated with 30 μM (orange) or 85 μM (blue) U(VI) for 7 days together with an original spectrum from cryo-time-resolved laser-induced fluorescence spectroscopy of a sample incubated with 30 μM U(VI) for 5 h (black), and (b) the cryo fluorescence microscopic images.

30 μM U(VI) Incubations. The results in this study showed that the formation of U(VI) phosphate minerals depends on the initial uranium concentration. At a lower initial uranium concentration of 30 μM, U(VI) phosphate minerals represented by meta-autunite group account for the major fraction at any incubation time. The precipitation of U(VI)-phosphate minerals by Archaea was previously reported only for a few species, namely *Metallosphaera sedula* and *Sulfolobus acidocaldarius*.[12,13] The formation of ammonium uranyl phosphate trihydrate $(NH_4UO_2PO_4(H_2O)_3)$ was shown for *M. sedula* with U_3O_8 as uranium substrate under chemolithoautotrophic conditions.[13] *S. acidocaldarius* precipitated U(VI) phosphate mineral phases only at pH 6, but not at pH 4.5, which is more favorable for them.[12] The association of uranium with *H. salinarum* ATCC 43214^T resulted in the formation of extracellular uranium

DOI: 10.1021/acs.est.8b02667
Environ. Sci. Technol. 2018, 52, 12895−12904

containing dense deposits, indicating that U(VI) was predominantly complexed with cellular inorganic phosphate.[11] Bacteria can release inorganic phosphate during starvation or under stress and thus mineralize high amounts of uranium.[6,11] It was demonstrated that, in comparison to many other microorganisms, cells of the archeon *Halobacterium salinarium* strain ET 1001 store phosphates mainly as magnesium orthophosphate rather than polyphosphates.[47] Such inorganic phosphates could contribute to the mineralization of uranium. Another potential source of inorganic phosphate is extracellular DNA, which was detected in biofilm structures of *H. salinarum* DSM 3754^T.[35] The members of the family *Halobacteriaceae* can use the extracellular DNA as a phosphorus source.[48−50] It was also shown that extracellular DNA from bacterial extracellular polymeric substances (EPS) contributes to uranium biomineralization.[51] The extracellular DNA can be released when cells lyse due to toxic effects. Due to the high salinity, the measurement of phosphate released by *H. noricense* DSM 15987^T was technically not possible and, hence, the active release of inorganic phosphate by *H. noricense* DSM 15987^T for uranium biomineralization could not be proven. For future experiments, proteomic analysis can be used to get information about the phosphate metabolism during exposure to uranium as demonstrated for *Microbacterium oleivorans* A9 that biomineralize uranium in autunite-like mineral phases.[52]

The multistage association behavior observed at the lower initial uranium concentration of 30 μM includes an association of U(VI) to the archaeal cells and potentially the formation of U(IV)-carbonate at the beginning, which is followed by a partial release of U(VI) presumably due to a protective mechanism of the cells. Finally, this further followed an increased association of U(VI) via the formation of U(VI) phosphate minerals and the association with a polynuclear lactate-like structure, which decreased the uranium content in the supernatant. A similar multistage association of uranium was shown for *Halobacterium noricens* DSM 15987^T also with 40 μM U(VI)[53] and for a *Microbacterium* isolate from Chernobyl.[54]

85 μM U(VI) Incubations. At a higher initial uranium concentration of 85 μM, the cells agglomerated immediately. It has been recently reported that biofilm structures attached to glass were formed by cells of *H. salinarum* DSM 3754^T.[35] Furthermore, Kawakami and colleagues observed that divalent/trivalent cations (Ca(II), Cr(II), Mn(II), and Fe(III)) can initiate the cell aggregation by *Halobacterium salinarum* CCM 2090.[55] In this study, the viability of the cells was only slightly affected (above 90%) and the influence of different metal concentrations on the cell aggregation and cell viability was not systematically studied.[55] However, our results suggest that U(VI) can initiate the cell agglomeration of *H. noricense* DSM 15987^T, which is influenced by uranium concentration and incubation time.

At the higher initial uranium concentration of 85 μM, the EXAFS results reveal a higher fraction of U(VI) associated with a polynuclear lactate-like structure. Such carboxylate functional groups can be found in NANA as an α-hydroxy acid motif. NANA was detected as EPS in biofilm structures of *H. salinarum* DSM 3754^T[35] and is a part in certain glycoprotein species of archaeal S-layers components.[56,57] The higher fraction of U(VI) carboxylates represented as polynuclear lactate-like structure can result from the complexation of U(VI) with organic molecules released by lysed cells because of toxic effects at the used higher uranium concentration. In accordance to the results obtained from EXAFS, the complexation of U(VI) by carboxylate groups was proven by cryo-TRLFS (Figure 4). Due to the robust deconvolution of the extensive three-dimensional cryo-TRLFS data set of all luminescence measurements with PARAFAC, three different carboxylate species could be revealed. One spectrum (spectrum 3) could be assigned to a citrate-like structure. The spectra 4 and 5 show the typical loss of fine structure of polynuclear species, which is also present in the polynuclear 3:5 U(VI) hydroxo complex (spectrum 1 in Figure 4). This is the dominating aqueous uranyl species at the investigated pH. According to the spectra, the polynuclear structure motif is conserved in the formed biocomplexes. However, the absolute emission maxima are shifted to higher wavelength, due to complexation with carboxylate groups. Hence, it clearly demonstrates that the aquatic speciation affects metal interaction pathways.

The association of uranium with *H. salinarum* ATCC 43214^T was performed at a similar pH but with a higher uranium concentration of 125 μM (as uranyl nitrate), under anaerobic conditions only for 2 h and resulted in the formation of extracellular uranium containing dense deposits, indicating that U(VI) was predominantly complexed with cellular inorganic phosphate. In comparison, with similar conditions of 85 μM of initial uranium concentration and 1 h of incubation time, our study showed the formation of U(VI) phosphate minerals as a minor fraction and U(IV) species and U(VI) carboxylate species represent the major fractions instead. Discrepancy between our results and those in[11] could originate from the above-described differences in the experimental procedure as, for example, different initial uranium concentration and aeration conditions. Furthermore, *H. salinarum* and *H. noricense* belong to the same genus *Halobacterium* but these are two different species which may have different physiologies reflected in their response to uranium exposure.

Potential U(VI) Reduction. At the shortest incubation time of 1 h, a significant fraction of U(IV) was detected by XAS at both the lower and higher U(VI) concentrations. To the best of our knowledge, this is the first time that the reduction of U(VI) to U(IV) in the presence of a *Halobacterium* species was observed. Hitherto, the reduction of Fe(III) as well as U(VI) was reported only by the hyperthermophilic archaeon *Pyrobaculum islandicum*, where the reduction of U(VI) was dependent upon the presence of cells and hydrogen at 100 °C.[58] A variety of different bacteria also exhibit the capacity to reduce U(VI) to U(IV), forming crystalline uraninite or nonuraninite U(IV) phases.[59] In this study the formation of a U(IV) carbonate compound was shown in the presence of *H. noricense* DSM 15987^T. However, it cannot be fully excluded that the reduction of U(VI) to U(IV) is taking place in the sample holder under the experimental conditions. Another possibility would be that released metabolites from lysed cells could be involved in the U(VI) reduction. Further experiments are needed to clarify this.

Spectroscopic Tools. This study also demonstrated that synchrotron-based XAS combined with cryo-TRLFS is a powerful tool to study the uranium-microbe system owing to their sensitivity and elemental selectivity.[60] XAS would be more advantageous to simultaneously acquire information about the oxidation states and distribution of the chemical species in the samples without suffering from quenching effects or quantum yields that are significant issues in luminescence-based methods.[46] The luminescence decay as the additional third dimension of TRLFS data can be used for advanced multiway data analysis like PARAFAC.[38]

DOI: 10.1021/acs.est.8b02667
Environ. Sci. Technol. 2018, 52, 12895−12904

Environmental Implications. Regarding the safe storage of high level radioactive waste in a deep geological repository, where rock salt is a potential host rock, its migration after a potential release needs to be assessed in relation to microbial interactions as it has been demonstrated in the present study. The studied archaeon *H. noricense* DSM 15987^T, which is indigenous in rock salt, interacts with uranium in a complex manner. This interaction process can be described as a multistage process, which is influenced by a range of parameters such as uranium concentration and contact time. Depending on the uranium concentration, the interaction of the archaeon *H. noricense* with uranium would result in (1) the biomineralization of uranium to eventually form solid phases of U(VI), (2) the attachment of U(VI) in extracellular polymeric substances or to the components of the cell walls via their carboxylate groups, and/or (3) the potential reduction of U(VI) to U(IV) to eventually form solid U(IV) phases. All these possible pathways will lead to the transformation of soluble uranium into immobile phases. Hence, the presence of microbes such as *H. noricense* in the actual repository environment could potentially benefit the immobilization or retardation of uranium. The results obtained in this study suggest different pathways of U(VI) immobilization by microbes, having potential implications for the reliable assessment of the long-term migration behavior of redox-active radionuclides, such as uranium, in saline environments as well as for the development of specific engineered subsurface environments and associated bioremediation strategies. This study also highlights the potential involvement of Archaea in geochemical cycling and biomineralization of metals and radionuclides in hypersaline environments.

■ ASSOCIATED CONTENT

Supporting Information

The Supporting Information is available free of charge on the ACS Publications website at DOI: 10.1021/acs.est.8b02667.

Additional descriptions of materials and methods, micrographs as well as spectra and analysis of XAS and TRLFS not shown in the main text (PDF)

■ AUTHOR INFORMATION

Corresponding Author

*Phone: +49(0)3512602989; e-mail: a.cherkouk@hzdr.de.

ORCID

Atsushi Ikeda-Ohno: 0000-0003-3380-5211

Andrea Cherkouk: 0000-0002-3908-2539

Notes

The authors declare no competing financial interest.

■ ACKNOWLEDGMENTS

We thank Sabrina Gurlit and Stefanie Schubert for ICP-MS measurements and Monika Dudek, Katrin Flemming and Sindy Kluge for technical assistance. We are grateful for using the analytical facilities of the Centre for Chemical Microscopy (ProVIS) at the Helmholtz Centre for Environmental Research, which is supported by European Regional Development Funds (EFRE - Europe funds Saxony) and the Helmholtz Association. We thank Andreas Massanek from the Geoscientific Collections of the TU Bergakademie Freiberg for providing us meta-autunite for reference measurements.

■ REFERENCES

(1) Lindley, B. A.; Fiorina, C.; Gregg, R.; Franceschini, F.; Parks, G. T. The effectiveness of full actinide recycle as a nuclear waste management strategy when implemented over a limited timeframe - Part I: Uranium fuel cycle. *Prog. Nucl. Energy* **2015**, *85*, 498−510.

(2) Swanson, J. S.; Cherkouk, A.; Arnold, T.; Meleshyn, A.; Reed, D. T. *The Microbiology of Subsurface, Salt-Based Nuclear Waste Repositories:Using Microbial Ecology, Bioenergetics, And Projected Conditions to Help Predict Microbial Effects on Repository Performance, LA-UR-16−28895*; Los Alamos National Laboratory, 2016.

(3) Jaakkola, S. T.; Ravantti, J. J.; Oksanen, H. M.; Bamford, D. H. Buried alive: Microbes from ancient halite. *Trends Microbiol.* **2016**, *24*, 148−160.

(4) Swanson, J. S.; Reed, D. T.; Ams, D. A.; Norden, D.; Simmons, K. A. *Status Report on the Microbial Characterization of Halite and Groundwater Samples from the WIPP, LA-UR-12−22824*; Los Alamos National Laboratory, 2012.

(5) Lloyd, J. R.; Macaskie, L. E., Biochemical basis of microbe-radionuclide interactions. In *Interactions of Microorganisms with Radionuclides*; Keith-Roach, M. J.; Livens, F. R., Eds.; Elsevier Science: 2002; *Vol. 2*, pp 313−342.

(6) Selenska-Pobell, S.; Merroun, M., Accumulation of heavy metals by microorganisms: biomineralization and nanocluster formation. In *Prokaryotic Cell Wall Compounds - Structure and Biochemistry*; H., König, Claus, H., Varma, A., Eds.; Springer: Heidelberg, 2010; pp 483−500.

(7) Jones, D. L.; Andrews, M. B.; Swinburne, A. N.; Botchway, S. W.; Ward, A. D.; Lloyd, J. R.; Natrajan, L. S. Fluorescence spectroscopy and microscopy as tools for monitoring redox transformations of uranium in biological systems. *Chem. Sci.* **2015**, *6* (9), 5133−5138.

(8) Beazley, M. J.; Martinez, R. J.; Sobecky, P. A.; Webb, S. M.; Taillefert, M. Uranium biomineralization as a result of bacterial phosphatase activity: Insights from bacterial isolates from a contaminated subsurface. *Environ. Sci. Technol.* **2007**, *41* (16), 5701−5707.

(9) Merroun, M. L.; Nedelkova, M.; Ojeda, J. J.; Reitz, T.; Fernandez, M. L.; Arias, J. M.; Romero-Gonzalez, M.; Selenska-Pobell, S. Bio-precipitation of uranium by two bacterial isolates recovered from extreme environments as estimated by potentiometric titration, TEM and X-ray absorption spectroscopic analyses. *J. Hazard. Mater.* **2011**, *197*, 1−10.

(10) Liang, X. J.; Hillier, S.; Pendlowski, H.; Gray, N.; Ceci, A.; Gadd, G. M. Uranium phosphate biomineralization by fungi. *Environ. Microbiol.* **2015**, *17* (6), 2064−2075.

(11) Francis, A. J.; Gillow, J. B.; Dodge, C. J.; Harris, R.; Beveridge, T. J.; Papenguth, H. W. Uranium association with halophilic and non-halophilic bacteria and archaea. *Radiochim. Acta* **2004**, *92* (8), 481−488.

(12) Reitz, T. U(VI) bioaccumulation by *Paenibacillus* sp. JG-TB8 and *Sulfolobus acidocaldarius*; Au(0) nanoclusters formation on the S-layer of S. acidocaldarius. PhD thesis, TU Dresden, 2011.

(13) Mukherjee, A.; Wheaton, G. H.; Blum, P. H.; Kelly, R. M. Uranium extremophily is an adaptive, rather than intrinsic, feature for extremely thermoacidophilic *Metallosphaera* species. *Proc. Natl. Acad. Sci. U. S. A.* **2012**, *109* (41), 16702−16707.

(14) Ozaki, T.; Gillow, J. B.; Kimura, T.; Ohnuki, T.; Yoshida, Z.; Francis, A. J. Sorption behavior of europium(III) and curium(III) on the cell surfaces of microorganisms. *Radiochim. Acta* **2004**, *92* (9−11), 741−748.

(15) Ventosa, A.; Oren, A. *Halobacterium salinarum* nom corrig, a name to replace *Halobacterium salinarium* (Elazari-Volcani) and to include *Hallobacterium halobium* and *Halobacterium cutirubrum*. *Int. J. Syst. Bacteriol.* **1996**, *46* (1), 347−347.

(16) Voica, D. M.; Bartha, L.; Banciu, H. L.; Oren, A. Heavy metal resistance in halophilic Bacteria and Archaea. *FEMS Microbiol. Lett.* **2016**, *363* (14), fnw146.

(17) Gruber, C.; Legat, A.; Pfaffenhuemer, M.; Radax, C.; Weidler, G.; Busse, H. J.; Stan-Lotter, H. *Halobacterium noricense* sp nov., an

archaeal isolate from a bore core of an alpine Permian salt deposit, classification of *Halobacterium* sp. NRC-1 as a strain of *H. salinarum* and emended description of *H. salinarum*. *Extremophiles* **2004**, *8* (6), 431−439.
(18) Gramain, A.; Diaz, G. C.; Demergasso, C.; Lowenstein, T. K.; McGenity, T. J. Archaeal diversity along a subterranean salt core from the Salar Grande (Chile). *Environ. Microbiol.* **2011**, *13* (8), 2105−2121.
(19) Jaakkola, S. T.; Zerulla, K.; Guo, Q. G.; Liu, Y.; Ma, H. L.; Yang, C. H.; Bamford, D. H.; Chen, X. D.; Soppa, J.; Oksanen, H. M. Halophilic archaea cultivated from surface sterilized middle-late eocene rock salt are polyploid. *PLoS One* **2014**, *9* (10), No. e110533.
(20) Jaakkola, S. T.; Pfeiffer, F.; Ravantti, J. J.; Guo, Q. G.; Liu, Y.; Chen, X. D.; Ma, H. L.; Yang, C. H.; Oksanen, H. M.; Bamford, D. H. The complete genome of a viable archaeum isolated from 123-million-year-old rock salt. *Environ. Microbiol.* **2016**, *18* (2), 565−579.
(21) Borkowski, M.; Lucchini, J.-F.; Richmann, M. K.; Reed, D. T. *Actinide (III) Solubility in WIPP Brine: Data Summary and Recommendations, LA-14360*; Los Alamos National Laboratory: 2009.
(22) Ams, D. A.; Swanson, J. S.; Szymanowski, J. E. S.; Fein, J. B.; Richmann, M.; Reed, D. T. The effect of high ionic strength on neptunium (V) adsorption to a halophilic bacterium. *Geochim. Cosmochim. Acta* **2013**, *110*, 45−57.
(23) Opel, K.; Weiß, S.; Hübener, S.; Zänker, H.; Bernhard, G. Study of the solubility of amorphous and crystalline uranium dioxide by combined spectroscopic methods. *Radiochim. Acta* **2007**, *95*, 143−149.
(24) Matz, W.; Schell, N.; Bernhard, G.; Prokert, F.; Reich, T.; Claussner, J.; Oehme, W.; Schlenk, R.; Dienel, S.; Funke, H.; Eichhorn, F.; Betzl, M.; Prohl, D.; Strauch, U.; Huttig, G.; Krug, H.; Neumann, W.; Brendler, V.; Reichel, P.; Denecke, M. A.; Nitsche, H. ROBL - a CRG beamline for radiochemistry and materials research at the ESRF. *J. Synchrotron Radiat.* **1999**, *6*, 1076−1085.
(25) Koningsberger, D. C.; Prins, R. *X-Ray Absorption: Principles, Applications, Techniques of EXAFS, SEXAFS and XANES*; Wiley, 1987.
(26) George, G. N.; Pickering, I. J. *EXAFSPAK, A Suite of Computer Programs for Analysis of X-ray Absorption Spectra*; Stanford, 2000.
(27) Ressler, T. WinXAS: a program for X-ray absorption spectroscopy data analysis under MS-Windows. *J. Synchrotron Radiat.* **1998**, *5*, 118−122.
(28) Drobot, B.; Bauer, A.; Steudtner, R.; Tsushima, S.; Bok, F.; Patzschke, M.; Raff, J.; Brendler, V. Speciation studies of metals in trace concentrations: the mononuclear uranyl(VI) hydroxo complexes. *Anal. Chem.* **2016**, *88*, 3548−3555.
(29) Günther, A.; Steudtner, R.; Schmeide, K.; Bernhard, G. Luminescence properties of uranium(VI) citrate and uranium(VI) oxalate species and their application in the determination of complex formation constants. *Radiochim. Acta* **2011**, *99*, 535−541.
(30) Andersson, C. A.; Bro, R. The n-way toolbox for MATLAB. *Chemom. Intell. Lab. Syst.* **2000**, *52* (1), 1−4.
(31) Grossmann, K.; Arnold, T.; Krawczyk-Bärsch, E.; Diessner, S.; Wobus, A.; Bernhard, G.; Krawietz, R. Identification of fluorescent U(V) and U(VI) microparticles in a multispecies biofilm by confocal laser scanning microscopy and fluorescence spectroscopy. *Environ. Sci. Technol.* **2007**, *41* (18), 6498−6504.
(32) Hennig, C.; Ikeda-Ohno, A.; Emmerling, F.; Kraus, W.; Bernhard, G. Comparative investigation of the solution species $[U(CO_3)_5]^{6-}$ and the crystal structure of $Na_6[U(CO_3)_5]\cdot 12H_2O$. *Dalton Trans* **2010**, *39* (15), 3744−3750.
(33) Ikeda-Ohno, A.; Hennig, C.; Tsushima, S.; Scheinost, A. C.; Bernhard, G.; Yaita, T. Speciation and structural study of U(IV) and -(VI) in perchloric and nitric acid solutions. *Inorg. Chem.* **2009**, *48* (15), 7201−7210.
(34) Malinowski, E. R. *Factor Analysis in Chemistry*, 3rd ed.; Wiley, 2002.
(35) Fröls, S.; Dyall-Smith, M.; Pfeifer, F. Biofilm formation by haloarchaea. *Environ. Microbiol.* **2012**, *14* (12), 3159−3174.
(36) Lucks, C. Untersuchungen zur Struktur von wassergelösten und an Hämatit sorbierten Uran(VI)-Komplexen mit aliphatischen (Hydroxy-) Carbonsäuren: Kombination verschiedener spektroskopischer Methoden mit Faktorenanalyse und quantenchemischen Berechnungen. PhD thesis, TU Dresden, 2013.
(37) Grenthe, I.; Drozdzynski, J.; Fujino, T.; Buck, E. C.; Albrecht-Schmitt, T. E.; Wolf, S. F. Uranium. In *The Chemistry of the Actinide and Transactinide Elements (Set Vol.1−6)*; Morss, L. R.; Edelstein, N.; Fuger, J.; Katz, J. J., Eds., 2011; pp 253−698.
(38) Drobot, B.; Steudtner, R.; Raff, J.; Geipel, G.; Brendler, V.; Tsushima, S. Combining luminescence spectroscopy, parallel factor analysis and quantum chemistry to reveal metal speciation - a case study of uranyl(VI) hydrolysis. *Chem. Sci.* **2015**, *6* (2), 964−972.
(39) Steudtner, R.; Arnold, T.; Geipel, G.; Bernhard, G. Fluorescence spectroscopic study on complexation of uranium(VI) by glucose: a comparison of room and low temperature measurements. *J. Radioanal. Nucl. Chem.* **2010**, *284* (2), 421−429.
(40) Wang, Z. M.; Zachara, J. M.; Yantasee, W.; Gassman, P. L.; Liu, C. X.; Joly, A. G. Cryogenic laser induced fluorescence characterization of U(VI) in hanford vadose zone pore waters. *Environ. Sci. Technol.* **2004**, *38* (21), 5591−5597.
(41) Steudtner, R.; Sachs, S.; Schmeide, K.; Brendler, V.; Bernhard, G. Ternary uranium(VI) carbonato humate complex studied by cryo-TRLFS. *Radiochim. Acta* **2011**, *99*, 687−692.
(42) Guillaumont, R.; Fanghänel, T.; Fuger, J.; Grenthe, I.; Neck, V.; Palmer, D. A.; Rand, M. H., Update on the chemical thermodynamics of uranium, neptunium, plutonium, americium and technetium. *Chemical Thermodynamics***2003**, *5*.
(43) Zheng, Y. Z.; Tong, M. L.; Chen, X. M. Synthesis, structure and photoluminescent studies of two novel layered uranium coordination polymers constructed from UO(OH) polyhedra and pyridinedicarboxylates. *Eur. J. Inorg. Chem.* **2005**, *20*, 4109−4117.
(44) Liao, Z. L.; Li, G. D.; Wei, X.; Yu, Y.; Chen, J.-S. Construction of three-dimensional uranyl-organic frameworks with benzenetricarboxylate ligands. *Eur. J. Inorg. Chem.* **2010**, *24*, 3780−3788.
(45) Jiang, Y. S.; Yu, Z. T.; Liao, Z. L.; Li, G. H.; Chen, J. S. Syntheses and photoluminescent properties of two uranyl-containing compounds with extended structures. *Polyhedron* **2006**, *25* (6), 1359−1366.
(46) Wang, Z. M.; Zachara, J. M.; McKinley, J. P.; Smith, S. C. Cryogenic laser induced U(VI) fluorescence studies of a U(VI) substituted natural calcite: Implications to U(VI) speciation in contaminated Hanford sediments. *Environ. Sci. Technol.* **2005**, *39* (8), 2651−2659.
(47) Smirnov, A. V.; Suzina, N. E.; Kulakovskaya, T. V.; Kulaev, I. S. Magnesium orthophosphate, a new form of reserve phosphate in the halophilic archaeon *Halobacterium salinarium*. *Microbiology* **2002**, *71* (6), 677−683.
(48) Chimileski, S.; Dolas, K.; Naor, A.; Gophna, U.; Papke, R. T. Extracellular DNA metabolism in *Haloferax volcanii*. *Front. Microbiol.* **2014**, *5*, 57.
(49) Zerulla, K.; Chimileski, S.; Nather, D.; Gophna, U.; Papke, R. T.; Soppa, J. DNA as a phosphate storage polymer and the alternative advantages of polyploidy for growth or survival. *PLoS One* **2014**, *9* (4), No. e94819.
(50) Oren, A. DNA as genetic material and as a nutrient in halophilic Archaea. *Front. Microbiol.* **2014**, *5*, 539.
(51) Hufton, J.; Harding, J. H.; Romero-Gonzalez, M. E. The role of extracellular DNA in uranium precipitation and biomineralisation. *Phys. Chem. Chem. Phys.* **2016**, *18* (42), 29101−29112.
(52) Gallois, N.; Alpha-Bazin, B.; Ortet, P.; Barakat, M.; Piette, L.; Long, J.; Berthomieu, C.; Armengaud, J.; Chapon, V. Proteogenomic insights into uranium tolerance of a Chernobyl's *Microbacterium* bacterial isolate. *J. Proteomics* **2018**, *177*, 148−157.
(53) Bader, M.; Müller, K.; Foerstendorf, H.; Drobot, B.; Schmidt, M.; Musat, N.; Swanson, J. S.; Reed, D. T.; Stumpf, T.; Cherkouk, A. Investigation of U(VI) bioassociation onto an extremely halophilic archaeon. *J. Hazard. Mater.* **2017**, *327*, 225−232.
(54) Theodorakopoulos, N.; Chapon, V.; Coppin, F.; Floriani, M.; Vercouter, T.; Sergeant, C.; Camilleri, V.; Berthomieu, C.; Fevrier, L. Use of combined microscopic and spectroscopic techniques to reveal

DOI: 10.1021/acs.est.8b02667
Environ. Sci. Technol. 2018, 52, 12895−12904

interactions between uranium and Microbacterium sp A9, a strain isolated from the Chernobyl exclusion zone. *J. Hazard. Mater.* **2015**, *285*, 285−293.
(55) Kawakami, Y.; Hayashi, N.; Ema, M.; Nakayama, M. Effects of divalent cations on *Halobacterium salinarum* cell aggregation. *J. Biosci. Bioeng.* **2007**, *104* (1), 42−46.
(56) Albers, S. V.; Meyer, B. H. The archaeal cell envelope. *Nat. Rev. Microbiol.* **2011**, *9* (6), 414−426.
(57) Klingl, A. S-layer and cytoplasmic membrane - exceptions from the typical archaeal cell wall with a focus on double membranes. *Front. Microbiol.* **2014**, *5*, 624.
(58) Kashefi, K.; Lovley, D. R. Reduction of Fe(III), Mn(IV), and toxic metals at 100 degrees C by *Pyrobaculum islandicum*. *Appl. Environ. Microbiol.* **2000**, *66* (3), 1050−1056.
(59) Stylo, M.; Alessi, D. S.; Shao, P. P.; Lezama-Pacheco, J. S.; Bargar, J. R.; Bernier-Latmani, R. Biogeochemical controls on the product of microbial U(VI) reduction. *Environ. Sci. Technol.* **2013**, *47* (21), 12351−12358.
(60) Tan, X. L.; Fang, M.; Wang, X. K. Sorption speciation of lanthanides/actinides on minerals by TRLFS, EXAFS and DFT studies: a review. *Molecules* **2010**, *15* (11), 8431−8468.

DOI: 10.1021/acs.est.8b02667
Environ. Sci. Technol. 2018, 52, 12895−12904